LANGMUIR Article
Cite This: *Langmuir* 2018, 34, 2890−2899
pubs.acs.org/Langmuir

Flow-Driven Assembly of Microcapsules into Three-Dimensional Towers

Henry Shum*,† and Anna C. Balazs*,‡

†Department of Applied Mathematics, University of Waterloo, Waterloo, Ontario N2L 3G1, Canada
‡Department of Chemical & Petroleum Engineering, University of Pittsburgh, Pittsburgh, Pennsylvania 15261, United States

Supporting Information

ABSTRACT: By harnessing biochemical signaling and chemotaxis, unicellular slime molds can aggregate on a surface to form a long, vertical stalk. Few synthetic systems can self-organize into analogous structures that emerge out of the plane. Through computational modeling, we devise a mechanism for assembling tower-like structures using microcapsules in solution as building blocks. In the simulations, chemicals diffusing from a central patch on a surface produce a concentration gradient, which generates a radially directed diffusioosmotic flow along the surface toward the center. This toroidal roll of a fluid pulls the microcapsules along the surface and lifts them above the patch. As more capsules are drawn toward the patch, some units are pushed off the surface but remain attached to the central microcapsule cluster. The upward-directed flow then draws out the cluster into a tower-like shape. The final three-dimensional (3D) structure depends on the flow field, the attractive capsule−capsule and capsule−surface interaction strengths, and the sedimentation force on the capsules. By tuning these factors, we can change the height of the structures that are produced. Moreover, by patterning the areas of the wall that are attractive to the capsules, we can form multiple vertical strands instead of a single tower. Our approach for flow-directed assembly can permit the growth of reconfigurable, 3D structures from simple subunits.

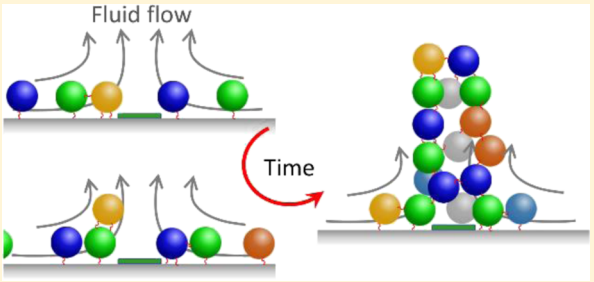

1. INTRODUCTION

The simple slime mold *Dictyostelium discoideum* can undergo a remarkable form of collective behavior and self-organization. The process is initiated by individual cells emitting a chemical signal into their surroundings. Neighboring cells sense this signal and respond by moving toward high concentrations of the chemical (i.e., chemotaxing). In this manner, the unicellular organisms aggregate into extensive two-dimensional (2D) clusters. Subsequently, the assembled cells self-organize into a tall, vertical structure that extends upward from the initially formed 2D aggregate. These vital processes are enabled by the inherent biochemical machinery in the living organisms. There are few synthetic systems that can match this level of concerted communication and dynamic, three-dimensional (3D) structure formation. The challenge in achieving analogous modes of self-organization with man-made materials is to replace the intrinsic instruction set provided by biology with the appropriate external cues, which can couple to the properties of the material to effectively direct their behavior.

Herein, we devise a mechanism that enables simple microcapsules to emulate salient features of the structure formation seen with the unicellular slime mold. Rather than employing cell signaling, we utilize a chemical-releasing patch in solution to generate chemical gradients. Instead of relying on the cell motility, we use the chemical gradients to generate fluid flows, which transport the capsules. Finally, we introduce attractive interactions between the capsules and between the capsules and a surface to regulate the structure formation.

To carry out these studies, we develop theoretical and computational models for the behavior of microcapsules in dynamically evolving flow fields. In previous studies,[1−5] we exploited the interactions between microcapsules, surfaces, and the surrounding fluid to drive the self-organization of the capsules into complex 2D, dynamic assemblies. We now specifically focus on harnessing diffusioosmosis in a fluid-filled chamber to achieve the desired 3D structure formation. To explain the phenomenon of diffusioosmosis, it is useful to first describe electroosmosis. Indeed, it was demonstrated over 200 years ago that an applied electric field could cause water to migrate through a porous material.[6] This migration, known as electroosmosis, is caused by phenomena occurring at the interface between an electrolytic solution and a material that carries a net surface charge when exposed to water; glass, for example, is negatively charged with a zeta potential $\zeta \approx -60$ mV, depending on the solution.[7,8]

Electroosmosis has been studied extensively in theory and experiments.[8−12] Briefly, the charged solid wall attracts counterions in the solution into a diffuse layer close to the interface. An externally applied electric field results in a force on

Received: November 26, 2017
Revised: January 26, 2018
Published: January 29, 2018

DOI: 10.1021/acs.langmuir.7b04051
Langmuir 2018, 34, 2890−2899

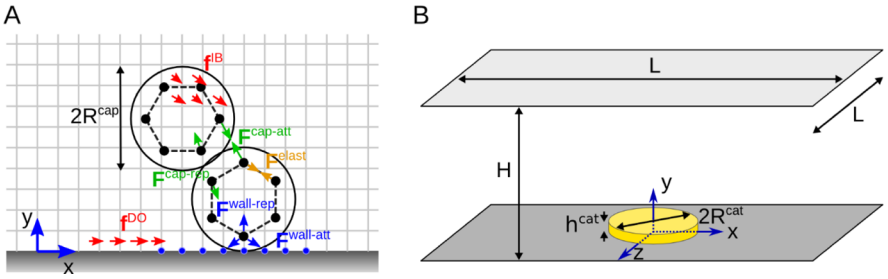

Figure 1. Schematic of the model setup. (A) A 2D representation of forces acting on the fluid and two capsules. Actual simulations are performed in a 3D domain with a higher spatial resolution. The fluid flow is solved on a grid (light gray) via a lattice Boltzmann method. Forces acting on the fluid (red) include the diffusioosmotic force $\mathbf{f}^{DO}$ at the bottom wall and forces $\mathbf{f}^{IB}$ exerted by the immersed boundaries of the capsules (mesh nodes indicated by the black dots). The capsules experience elastic forces and interactions with other capsules and with the wall (see text for details). (B) Computational domain (capsules not shown) bounded by walls on the top and bottom. Lateral boundaries are periodic. A disc-shaped region (yellow) on the bottom wall represents a catalytic patch that acts as a chemical source.

the counterions in the diffuse layer. If the electric field is parallel to the wall, then the force causes a sustained drift of counterions, and fluid, along the wall. This principle has been applied to drive fluid flows at speeds of the order of millimeters per second in microfluidic channels.[11,12] Because the driving force only acts in the thin boundary layer at the channel walls, the fluid flow velocity is spatially uniform outside this boundary layer. From a macroscopic perspective, electroosmosis produces an effective fluid slip velocity at the channel walls.

Similar fluid flows can also be generated when the electric field is not externally imposed but locally induced because of a gradient in the concentration C of an electrolyte in the solution[13−15]

$$\mathbf{E}^{\text{induced}} \approx \frac{kT}{Ze}\left[\beta - (1-\beta^2)\frac{Ze\psi}{kT}\right]\frac{\nabla C}{C}, \qquad \beta = \frac{D_+ - D_-}{D_+ + D_-} \tag{1}$$

where k is the Boltzmann constant, T is the temperature, Z is the electrolyte valence (assuming positive and negative ions have charges of an equal magnitude for simplicity), e is the elementary charge, ψ is the electrostatic potential, D_+ is the diffusion coefficient of the positive ions, and D_- is the diffusion coefficient of the negative ions.

The electrokinetic flow due to concentration gradients is known as diffusioosmosis. In addition to the electroosmotic effect described above, there is a "chemiosmotic" contribution that is present whether the solutes are charged (i.e., an electrolyte) or neutral. The overall diffusioosmotic flow speed outside the interfacial layer is approximated by[14]

$$\mathbf{u}^{DO} = \gamma\left(\frac{\nabla_{\parallel}C}{C}\right), \qquad \gamma = \frac{\varepsilon}{4\pi\eta}\left(\beta\zeta\frac{kT}{Ze} + \frac{1}{8}\zeta^2[1-2(1-\beta^2)]\right) \tag{2}$$

where $\nabla_{\parallel}C$ denotes the component of the concentration gradient parallel to the wall, ε is the permittivity, η is the viscosity of the fluid, and ζ is the zeta potential of the wall. We note that the flow speed is proportional to $(\nabla_{\parallel}C)/C$, and the constant of proportionality γ depends on the zeta potential of the wall, as well as other experimentally measurable factors. Diffusioosmotic flows with speeds up to 40 μm/s have been observed around dissolving particles of calcium carbonate.[16] Other physical or chemical processes that generate concentration gradients, such as a reaction occurring locally at an immobilized patch of an enzyme or a catalyst, also drive diffusioosmotic flows.[17−19] Researchers have in fact used such diffusioosmotic flows to direct the 2D assembly of colloids in solution.[20,21]

In addition to flow fields, we exploit attractive interactions between the capsules and the substrate, as well as the interparticle attraction. Experimentally, tunable capsule−wall attractions can be achieved by functionalizing the surfaces of the capsule and the wall with ligands and receptors[22] or electrostatically interacting polymers.[23,24] Such techniques can be employed to pattern spatially varying surface interactions, which we utilize in our simulations. The interparticle interactions can also be regulated by functionalizing the surface of the capsules.[24,25] Hence, the components necessary to physically realize the systems described below are experimentally accessible.

2. METHODOLOGY

2.1. Simulation of Capsules and Fluid Flows. The schematic in Figure 1 shows the components of our system: a host fluid, microcapsules, chemical concentration field, and solid, confining walls. The fluid flow is governed by the incompressible Navier−Stokes equations

$$\rho\left(\frac{\partial \mathbf{u}}{\partial t} + \mathbf{u}\cdot\nabla\mathbf{u}\right) = -\nabla p + \mu\nabla^2\mathbf{u} + \mathbf{f}, \qquad \nabla\cdot\mathbf{u} = 0 \tag{3}$$

where ρ is the fluid density, $\mathbf{u}$ is the fluid flow field, p is the pressure field, μ is the dynamic viscosity of the fluid, and $\mathbf{f}$ is a force field acting on the fluid. We consider two contributions of forces on the fluid, $\mathbf{f} = \mathbf{f}^{IB} + \mathbf{f}^{DO}$, as detailed further below. The first, $\mathbf{f}^{IB}$, is the force distribution arising from the coupling of the fluid to the motion of the microcapsules, as modeled through the immersed boundary (IB) method. The second force, $\mathbf{f}^{DO}$, is the diffusioosmotic force acting on a thin layer of fluid adjacent to the bottom surface of the chamber.

We numerically solve the fluid flow equations with a lattice Boltzmann method using the D3Q19 scheme.[26−29] The computational grid size is $L \times H \times L$ with the horizontal length $L = 150$ and vertical height $H = 75$ in most simulations. The physical length scale of the grid spacing is set to $\Delta x = 1$ μm. We prescribe the periodic boundary conditions in the horizontal (x, z) directions and use the bounce-back technique to simulate no-slip conditions on the lower and upper (y) walls for the lattice Boltzmann fluid.[27]

DOI: 10.1021/acs.langmuir.7b04051
Langmuir 2018, 34, 2890−2899

Microcapsules are simulated using the IB method.[30−32] The IB for each capsule consists of a network of $N^{node} = 66$ mesh nodes distributed on a spherical surface of radius $R^{mesh} = 3.5\Delta x$, where Δx is the grid spacing associated with the Cartesian fluid lattice in both the IB method and the lattice Boltzmann method. In the IB algorithm, the mesh nodes are advected with the local fluid flow using a weighted average of velocity values at the nearby lattice sites. This procedure gives a single node a finite effective hydrodynamic radius $a^{eff} \approx 1.5\Delta x$,[33] resulting in an effective capsule radius larger than the mesh shell radius, $R^{cap} = 5\Delta x = 5\ \mu$m. The IB nodes influence the fluid flow by exerting forces on the fluid. These forces consist of contributions due to the elastic dynamics of the capsule, attractive and repulsive forces between the capsules, attractive and repulsive interactions with the wall, and gravity. Below, we discuss each of these forces in turn.

Elastic bonds between the neighboring mesh nodes exert forces $\mathbf{F}^{elast}$ when the nodes are perturbed from the equilibrium structure, maintaining an approximately spherical configuration of the capsule. Here, we assume that the capsules are sufficiently rigid that deformations are small.

To model intercapsule attractive interactions, for example, zwitterion dipole−dipole or van der Waals forces, we introduce a short-range, attractive force that acts between the nodes on different capsules. Each pairwise interaction force is modeled as the negative gradient of a Morse potential

$$\mathbf{F}^{cap\text{-}att} = -\mathbf{e}_r \frac{dV^{cap\text{-}att}}{dr},$$
$$V^{cap\text{-}att}(r) = A^{cap\text{-}att}[1 - \exp\{-\lambda^{cap\text{-}att}(r - r_e^{cap\text{-}att})\}]^2 \quad (4)$$

where r is the distance between a pair of interacting nodes, $r_e^{cap\text{-}att}$ is the equilibrium separation, $A^{cap\text{-}att}$ characterizes the strength of the Morse interaction, and $\lambda^{cap\text{-}att}$ determines the width or range of interactions. We fix the parameters $r_e^{cap\text{-}att} = 2a^{eff} = 3\Delta x$ and $\lambda^{cap\text{-}att} = 5\Delta x^{-1}$ and define a reference value for the potential strength $A_0 = 0.005$. The attractive force only acts when $r > r_e^{cap\text{-}att}$. When nodes of two capsules are closer together than the equilibrium separation, $r < r_e^{cap\text{-}att} = r_e^{cap\text{-}rep}$, a repulsive force acts between the nodes. This force is of the same form as eq 4 but with parameters labeled with a superscript "cap-rep" instead of "cap-att." In all simulations, we use the values $A^{cap\text{-}rep} = A_0$ and $\lambda^{cap\text{-}rep} = \lambda^{cap\text{-}att}$.

An analogous model is used for attractive interactions with the wall below the capsules. Specifically, we consider a square lattice of nodes on the wall, with spacing $\delta x = 0.5\Delta x$. Some of these nodes are removed to model regions with no capsule−wall attraction, as described for the respective simulations. The parameters defining the capsule−wall attraction $\mathbf{F}^{wall\text{-}att}$ are the same as in eq 4 but are denoted with a superscript "wall-att" instead of "cap-att."

A repulsive interaction is present at all points on the wall to prevent capsules from penetrating the boundary. The repulsive force on a node with a vertical position y is given by

$$\mathbf{F}^{wall\text{-}rep} = -\mathbf{e}_y \frac{dV^{wall\text{-}rep}}{dy},$$
$$V^{wall\text{-}rep}(y) = A^{wall\text{-}rep}$$
$$[1 - \exp\{-\lambda^{wall\text{-}rep}(y - y_e^{wall\text{-}rep})\}]^2 \quad (5)$$

with parameter values $y_e^{wall\text{-}rep} = a^{eff} = 1.5\Delta x$, $\lambda^{wall\text{-}rep} = 5\Delta x^{-1}$, and $A^{wall\text{-}rep} = 0.02$.

In certain simulations, we add a constant gravitational force $\mathbf{F}^{grav} = -(f^{grav}/N^{node})\mathbf{e}_y$ on each capsule node to model the sedimentation of the capsule. The total gravitational force acting on the capsule f^{grav} is proportional to the density excess relative to the surrounding fluid.

At low Reynolds numbers, inertia may be neglected, so we consider the sum of all forces discussed above to be balanced by the hydrodynamic (drag) force $\mathbf{F}^{hyd}$ on each capsule node

$$\mathbf{F}^{hyd} + \Sigma\mathbf{F}^{elast} + \Sigma\mathbf{F}^{cap\text{-}att} + \Sigma\mathbf{F}^{cap\text{-}rep} + \Sigma\mathbf{F}^{wall\text{-}att} + \mathbf{F}^{wall\text{-}rep} + \mathbf{F}^{grav} = 0 \quad (6)$$

where the Σ symbols denote summations over the relevant contributions. Following the procedures of the IB method, an opposite hydrodynamic force $-\mathbf{F}^{hyd}$ is transmitted to the fluid lattice points near the IB node; the lattice force distribution $\mathbf{f}^{IB}$ arises from the contributions of all capsule nodes.

The diffusioosmotic force $\mathbf{f}^{DO}$ acts on the fluid in the first layer of lattice nodes adjacent to the lower wall of the domain. On the basis of the effective diffusioosmotic slip velocity, eq 2, we define the diffusioosmotic force on the fluid by

$$\mathbf{f}^{DO} = \alpha \frac{\nabla_{\parallel} C}{C} \quad (7)$$

where $\nabla_{\parallel} C = (\partial_x C, 0, \partial_z C)^T$. Here, we set $\alpha = 0.01$, resulting in a maximum flow speed $u^{max} \approx 0.004$ in the lattice Boltzmann units $(\Delta x/\Delta t)$. We set the time step size $\Delta t = 0.1$ ms to match the magnitude of simulated flow fields to diffusioosmotic flow speeds observed in experiments.[16] Note that the lattice Boltzmann algorithm interrelates the kinematic viscosity of the fluid ν with the spatial and temporal step sizes. With our values of Δx and Δt, the simulated fluid viscosity is lower than that of water. The kinematics of the fluid and capsules are unaffected by this discrepancy, however, because the Reynolds number $Re = 2R^{cap}u^{max}/\nu < 1$ is small and in the low Reynolds number limit (Stokes flow), velocities simply scale linearly with forces.

A remark is warranted about the approach described above for modeling interactions between pairs of capsules and between a capsule and a wall. The total interaction is computed as a sum of contributions between pairs of nodes on nearby objects. This treatment is similar to the methods used in other numerical studies.[34−36] As the mesh becomes finer, so that the distance between the nodes of the same object decreases, the total interaction energy between the two objects approximates a double integral of an energy density that depends on the distance between the points on either object. This model for calculating interaction energies is known as the Hamaker summation method.[37]

Because of the discrete representation with nodes, however, the surfaces are effectively rough; a node of one capsule tends to be attracted to the "valleys" between the nodes of the wall or of an adjacent capsule. Hence, an attraction between the pairs of nodes causes some resistance to slip between the two surfaces, whereas computing the attraction based on the distance between centers of spherical capsules, for example, would allow the capsules to rotate freely relative to one another. Substantial tangential forces between particles have been measured experimentally in colloidal aggregates;[38] considering interactions between nodes is an effective approach

DOI: 10.1021/acs.langmuir.7b04051
Langmuir 2018, 34, 2890−2899

for modeling such tangential forces. The distance between nodes would be related to the "patchiness", or heterogeneity, of surface modifications responsible for interactions between the particles.[23]

We performed simulations to test whether the results of our model depend critically on our implementation of the close-range interactions. When interactions were computed based on the centers of the capsules and the perpendicular distance from walls instead of evaluating interactions between nodes, the capsules were still able to assemble into tower-like structures (see Video SV1). Thus, the assembly behavior observed in our simulations is robust to the treatment of attractive capsule−capsule and capsule−wall interactions. With the center-to-center model, however, capsules tend to rotate because of the fluid flow even when their positions within a cluster are stable.

2.2. Simulation of Chemical Concentration Fields. The chemical concentration field C in eq 7 is computed using the forward-time central-space finite difference method[3,39,40] to solve the diffusion equation

$$\frac{\partial C}{\partial t} = D\nabla^2 C + \phi \tag{8}$$

where D is the diffusion coefficient and ϕ is a spatially dependent source term. The same computational lattice is used as for the fluid flow. We do not consider the effects of advective transport in the evolution of the concentration field. This is justified in our model because we expect the Péclet number $Pe = 2R^{cat}U/D < 1$ to be low for flow speeds of the order of $U \approx 10\ \mu$m/s and typical diffusion coefficients for small ions $D \approx 1 \times 10^{-9}$ m^2/s.[16] We also assume that the chemical concentration field is unperturbed by the capsules. Hence, the concentration evolution is independent of the fluid flow and motion of the capsules.

We consider a simple reaction system whereby the chemical is produced at a constant rate per unit volume ϕ_0 within a thin, disc-shaped region (see Figure 1B), which represents a patch of a catalyst or an enzyme (radius $R^{cat} = 20\Delta x$, height $h^{cat} = \Delta x$) immobilized on the bottom surface. We assume that this catalyst produces the chemical components that cause diffusioosmosis. Periodic conditions are used for the horizontal boundaries, the no-flux condition $\partial C/\partial y = 0$ is imposed on the bottom wall ($y = 0$), and a constant concentration $C = C_0$, equal to the uniform initial concentration, is imposed on the top wall ($y = H$). The presence of other chemical species is neglected, but the effect of background solutes (such as pH buffers) on diffusioosmosis could be considered by raising the background concentration C_0.

Physically, the constant concentration boundary condition on the top wall implies that the chemical produced at the patch is removed from the system. We performed additional simulations replacing this condition with a no-flux boundary, which is experimentally simpler to achieve. The results were qualitatively the same except that the average concentration gradually increased as the chemical accumulated. This led to a gradual decay in the flow field because the diffusioosmotic flow is inversely proportional to the electrolyte concentration. In the model presented here, we assume that the time scale of this decay is sufficiently long (equivalently, the rate of chemical production is sufficiently low) that we can neglect this process. We therefore consider the constant concentration boundary condition on the top wall.

With the prescribed domain boundary conditions, the rate of chemical production at the patch is eventually balanced by the flux out of the domain and a steady concentration field is reached on the time scale $T^{diffusion} \approx H^2/D \approx 6$ s. Because this time is shorter than typical times for the assembly of the capsule structures ($T^{assembly} \approx 50$ s), we compute the equilibrium concentration field (decoupled from the fluid flow) once and use the result as a constant input to all simulations of fluid and capsule motion. We performed tests with the concentration field evolving simultaneously with the flow field and thereby confirmed that the initial transient evolution of the concentration field does not qualitatively affect the outcomes, that is, the assembly of towers.

2.3. Cluster Analysis for Quantifying the Tower Assembly. We characterize the outcomes of the simulations by analyzing the positions of the capsules at regular time intervals during the assembly process. The instantaneous configuration of capsules is analyzed as follows:

1. Capsules are classified as either "surface" or "bulk". Surface capsules are those with centers at a height less than $R^{thresh} = (R^{cap} + 0.1\Delta x)$ away from the bottom surface of the chamber. These capsules are considered to be in contact with the surface.
2. Bulk capsules are sorted into clusters by connectivity. Two capsules are considered to be directly connected if the distance between their centers is less than $l^{thresh} = (2R^{cap} + 0.1\Delta x)$. All capsules that are connected to each other either directly or through a series of direct connections are clustered together.
3. The largest cluster of bulk capsules that is connected to at least one surface capsule is identified. This cluster would be the tower, if one is present.
4. The cluster size N^C is defined as the number of capsules in the selected cluster, and the height of the cluster H^C is defined as the greatest y-position of capsules in the cluster. If there is no bulk cluster connected to a surface capsule, then $N^C = 0$ and H^C is undefined.
5. The number of remaining capsules $N^{remaining}$ is computed as the total number of capsules either in contact with the bottom surface or in a cluster that is connected to the surface.

The outcome of a given simulation is classified as one of three categories as follows:

1. "Detached" if, at any time, $N^{remaining}$ falls below half of the total number of capsules, N^{cap}. We use $N^{cap} = 60$ capsules in the analyzed simulations.
2. "Tower" if the clusters stabilize in shape and $N^C \geq 10$.
3. "Flat" if the clusters stabilize in shape and $N^C < 10$. Because capsules are not detached, this condition indicates that most of the capsules are in a monolayer on the surface of the chamber.

Simulations were run for 10^6 time steps, corresponding to 100 s of simulated time. Some were terminated early when it was determined that most of the capsules had detached. In cases where the shape of the tower was still evolving, simulations were continued beyond 10^6 time steps until the configuration of clusters became stable.

3. RESULTS

3.1. Diffusioosmotic Pumping. To generate a fluid flow that will aggregate microcapsules in a microfluidic chamber, we exploit the diffusioosmotic effect. We consider a thin, disc-shaped patch on the bottom of the chamber that acts as a chemical source (see Figure 1B). Several experimental setups

DOI: 10.1021/acs.langmuir.7b04051
Langmuir 2018, 34, 2890−2899

could be represented with this model; the source could be a thin piece of dissolving material,[16] a gel or resin that slowly releases a stored chemical species,[41−43] or a patch of an immobilized enzyme or a catalyst that locally drives a chemical reaction.[17,18,41,44] The concentration field and resulting flow field driven by diffusioosmosis on the bottom surface of the chamber are illustrated in Figure 2. Close to the bottom surface,

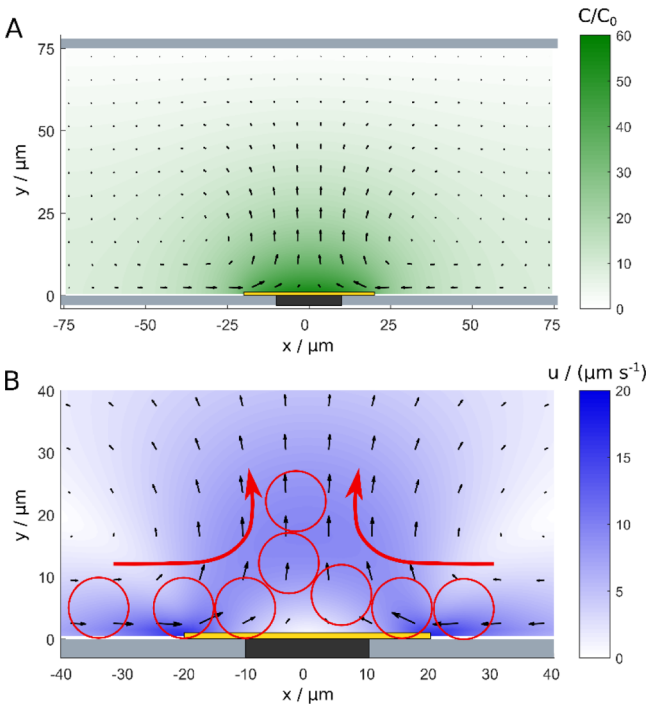

Figure 2. Concentration and fluid flow fields generated by the catalytic patch. (A) Concentration field in the vertical cross-section through the patch is represented by a heat map. The arrows indicate the direction and relative magnitude of the flow field. The catalytic patch is represented by a thin, yellow region, and the walls of the domain are depicted as light gray strips. The dark gray region on the bottom wall represents the portion of the surface that is nonattractive to the capsules. (B) Close-up of the catalytic patch with a heat map of the fluid flow speed in the vertical cross-section through the patch. The assembly of a tower, described in section 3.2, is depicted schematically. Capsules, represented by circular rings, move along the bottom wall but remain attached to the attractive, light gray regions. When the capsules are pushed onto the nonattractive, dark gray patch, they detach from the wall and rise.

the fluid flows toward the chemical source. Because the fluid is incompressible, there is an upward flow above the patch and the fluid circulates in a toroidal roll. This is the general form of the flow structure, provided the chamber is sufficiently large compared with the patch. Quantitatively, the flow field is affected by the diffusioosmotic constant γ in eq 2 and the background electrolyte concentration relative to the contribution from the chemical source.

To understand the role of the background concentration, let C^{patch} denote the concentration field due to the production at the patch and C_0 denote the background concentration such that the total electrolyte concentration is $C = C_0 + C^{patch}$. Because diffusion is a linear process, C^{patch} is proportional to the rate of production at the patch. Thus, we write $C^{patch} = C^*\tilde{C}^{patch}$, where C^* is the maximum value of C^{patch} in the domain (proportional to the rate of chemical production at the patch) and $\tilde{C}^{patch}$ is the rate-independent, rescaled field. The diffusioosmotic flow speed along the bottom surface, given in eq 2, is proportional to $(\nabla_\parallel C)/C = (\nabla_\parallel C^{patch})/(C_0 + C^{patch}) = (\nabla_\parallel \tilde{C}^{patch})/(C_0/C^* + \tilde{C}^{patch})$.

From the above expression, we deduce that the flow field depends on the ratio C_0/C^* but not the absolute concentration scale C^*. The patch is not required to produce a high absolute concentration of the electrolyte; low concentrations can generate diffusioosmotic flows as long as the background concentration is also low. Recent experiments[43] indeed demonstrated diffusioosmotic fluid pumping with estimated concentrations of the order of micromolar. Conversely, we remark that arbitrarily high flow speeds cannot be generated by simply increasing the rate of chemical production. Once C^* is much greater than the background electrolyte concentration, further increases in C^* will have a small effect on the flow speed. In our simulations, we set the constant chemical source term at the patch $\phi_0 = 0.1C_0/\Delta t$, which resulted in the ratio $C_0/C^* \approx 0.02$.

Because the fluid flow is one of the critical aspects controlling the assembly of clusters of capsules in our system, we emphasize that our simulated flow fields are consistent with the experimental observations of diffusioosmotic flows generated by chemical concentration gradients. Several experiments have reported the speeds and qualitative motion of tracer particles near diffusioosmotic pumps.[16−20] For example, Niu et al.[43] demonstrated that particles of an ion exchange resin generate diffusioosmotic flows in deionized water. The resin particles were 10−50 μm in radius, similar to the size of the catalytic patches we consider in our model system (R^{cat} = 20 μm in radius). Flow speeds close to the wall were inferred from the motion of polystyrene tracer particles 1.7−15.5 μm in diameter, comparable to the capsules in our model, $2R^{cap}$ = 10 μm.

The tracer particles were observed to move radially toward the resin pumps with speeds varying approximately as $1/r^\alpha$, where r is the distance between the tracer and the center of the pump and $1 \le \alpha \le 2$. We verified that our simulations reproduced this scaling behavior (up to distances approaching 75% of $L/2$, the midpoint between a pump and its periodic image in our computational model). In simulations, the exponent $1 \le a \le 2$ depended on the background electrolyte concentration C_0. In particular, $\alpha \approx 1$ when C_0 is insignificant compared with the concentration due to the reaction and $\alpha \approx 2$ when the chemical concentration from the reaction is insignificant compared with the background electrolyte concentration.

3.2. Formation of Towers of Microcapsules. Recall that our goal is to drive synthetic microcapsules to mimic salient features of the concerted self-organization observed in biological systems, that is, the 3D structure formation performed by unicellular slime molds. Hence, we aim to determine regions in phase space where the capsules can be directed to a central region on a surface and assembled into vertical structures that emerge out of the plane. Our objective of assembling microcapsules into 3D, tower-like structures was achieved by balancing diffusioosmotic flows and attractive capsule−wall and capsule−capsule interactions. We initialize N^{cap} = 60 capsules to be randomly distributed on the bottom (y = 0) wall of the chamber, ensuring that the capsules do not overlap with one another. Using the steady chemical concentration field computed, as described in section 2.2, we impose diffusioosmotic flow on the bottom wall. This drives the

DOI: 10.1021/acs.langmuir.7b04051
Langmuir 2018, 34, 2890−2899

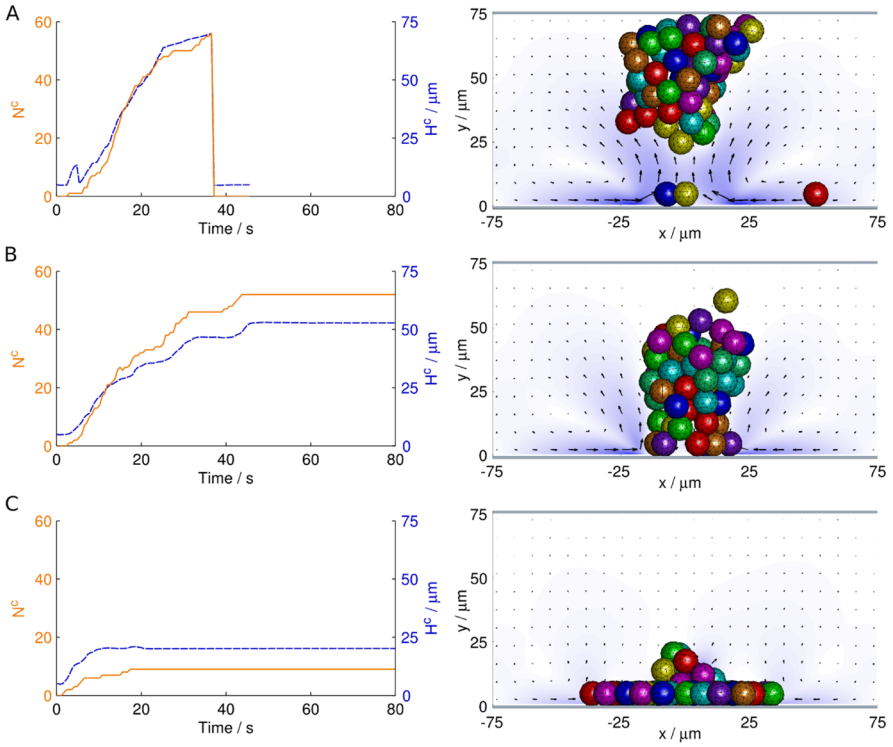

Figure 3. Assembly outcomes as the wall attraction strength is varied. Plots in the left-hand column show the time evolution of the wall-attached cluster size N^C (solid curves) and height H^C (dashed curves) defined in section 2.3. The final configurations of the capsules in the respective simulations are illustrated in the right-hand column. (A) $A^{\text{wall-att}} = 0.12A_0$. The capsules form a large cluster that detaches from the wall. (B) $A^{\text{wall-att}} = 0.16A_0$. The capsules form a tall tower that remains attached to the wall. (C) $A^{\text{wall-att}} = 0.32A_0$. A flat structure forms, with most of the capsules remaining in direct contact with the wall.

motion of the fluid throughout the chamber, and the capsules are advected with the flow toward the catalytic patch.

In the absence of gravity and attractive interactions between the capsules and the surface, the capsules would be lifted up by the fluid flow as they approach the patch. To prevent the capsules from detaching, we introduce the wall−capsule attraction described in section 2.1. The capsules must lift off from the surface once they reach the center of the patch, however, or a tower would not be formed. Hence, we designate a circular region of radius $R^{\text{lift}} = 10\Delta x$ with no capsule−wall attraction, located in the center of the catalytic patch. The diffusioosmotic fluid flow drives the capsules toward the center of the patch, but the capsules encounter an energy barrier at the interface between the attractive and nonattractive regions of the surface. As a result, the capsules tend to aggregate around the perimeter of the nonattractive patch. To build a tower, we require the capsules to remain attached to the surface until more capsules arrive at the patch. The new capsules should join at the base of the existing structure and push the tower up while keeping the tower anchored to the surface. This process is shown schematically in Figure 2B.

We deliberately chose the radius of the nonattractive patch to be smaller than that of the catalytic patch, $R^{\text{lift}} = R^{\text{cat}} - 2R^{\text{cap}}$. Because the horizontal fluid flow speed is greatest at the perimeter of the catalytic patch (see Figure 2B), incoming capsules are able to push the anchoring capsules onto the nonattractive patch, thereby detaching them from the surface.

For towers to form correctly, the strength of the capsule−wall attraction must be carefully controlled. In our simulations, we varied the depth of the Morse potential describing capsule−surface attractions (see section 2.1) from $A^{\text{wall-att}}/A_0 = 0.12$ to $A^{\text{wall-att}}/A_0 = 0.32$ in increments of 0.04. The strength of attractive capsule−capsule interactions was fixed at $A^{\text{cap-att}} = A_0$. Three representative simulations are shown in Figure 3. For the low value $A^{\text{wall-att}} = 0.12A_0$, the capsules aggregated at the patch and formed a large cluster that eventually detached from the bottom and rose to the top of the chamber (Figure 3A, Video SV2). A tall tower formed at the intermediate value $A^{\text{wall-att}} = 0.16A_0$ (Figure 3B, Video SV3), whereas a small mound surrounded by a flat, monolayer cluster formed when $A^{\text{wall-att}}$ was large (Figure 3C, Video SV4).

Because the outcome of a simulation with any given parameters could depend on the random initial positions of the capsules, we performed three independent runs with different initial capsule placements for each wall attraction strength. The mean cluster heights $\langle H^C \rangle$ were computed, and the overall behavior was determined by the outcome in the majority of runs for each value of $A^{\text{wall-att}}$. These results are plotted in Figure 4. In all three runs with the weakest wall attraction, the capsules detached, so $\langle H^C \rangle$ was undefined. Apart from this, the mean cluster height decreased as the capsule−wall attraction strength increased. Only in the case $A^{\text{wall-att}} = 0.16A_0$ did towers form robustly. For higher values of $A^{\text{wall-att}}$, the capsules formed flat clusters, as defined in section 2.3.

3.3. Effects of Sedimentation. In section 3.2, we neglected gravitational forces on the capsules. This assumption is appropriate if the density of the capsule is close to that of the surrounding fluid. If necessary, density matching can be achieved by adding glycerol to the solution.[43,45] To assess whether the formation of towers is robust to sedimentation effects, we introduced a gravitational force on the capsules. Other parameters were maintained as in the successful tower-

DOI: 10.1021/acs.langmuir.7b04051
Langmuir 2018, 34, 2890−2899

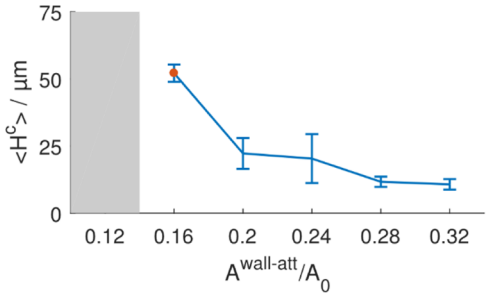

Figure 4. Dependence of the assembled cluster height on the wall attraction strength. The mean heights $\langle H^C \rangle$ are computed from three independent runs. Error bars represent one standard deviation above and below the mean. The circular marker at $A^{\text{wall-att}} = 0.16A_0$ indicates that the towers were robustly assembled in these simulations. With $A^{\text{wall-att}} = 0.12A_0$, the capsules detached, and for $A^{\text{wall-att}} \geq 0.2A_0$, flat structures formed.

forming case in section 3.2, with $A^{\text{wall-att}} = 0.16A_0$. As shown in Figure 5, towers still emerged, but the height of the towers

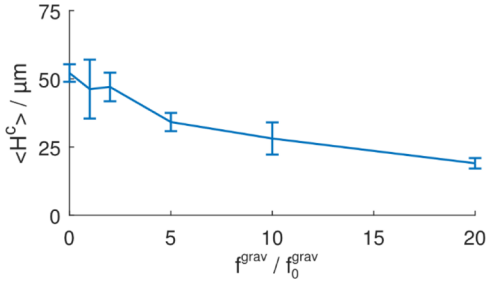

Figure 5. Dependence of mean tower height on the capsule sedimentation force f^{grav}. Error bars indicate one standard deviation, calculated from three runs. Towers formed in all cases, following the classification scheme in section 2.3. In these simulations, the capsule–wall attraction strength was $A^{\text{wall-att}} = 0.16A_0$. The data point at $f^{\text{grav}} = 0$ corresponds to the marked point in Figure 4.

decreased as the gravitational force was increased. The average cluster height was 52 μm without gravity and 19 μm with the gravitational force magnitude $f^{\text{grav}} = 20f_0^{\text{grav}}$. The reference value f_0^{grav} is defined such that the sedimentation speed of the capsule, according to Stokes' drag law, is

$$v_0^{\text{grav}} = \frac{f_0^{\text{grav}}}{6\pi\mu R^{\text{cap}}} = \frac{2}{9}\frac{g\Delta\rho}{\mu}(R^{\text{cap}})^2 = 0.64\ \mu\text{m s}^{-1} \quad (9)$$

where $\Delta\rho$ is the difference in density between the capsules and the surrounding fluid and g is the gravitational acceleration constant. This reference value corresponds to a capsule of density $\rho^{\text{cap}} = 1.01$ g cm^{-3} sedimenting in a dilute, aqueous medium. For comparison, polystyrene microparticles have a density of $\rho^{\text{ps}} = 1.05$ g cm^{-3}.[45] Hence, polystyrene microparticles would experience a sedimentation force $f^{\text{grav}} \approx 5f_0^{\text{grav}}$, for which our results suggest that tower formation could be possible.

3.4. Effects of Capsule–Capsule Attraction Strength. The formation of cohesive tower-like structures in the previous sections demonstrates that the intercapsule attraction strength $A^{\text{cap-att}} = A_0$ was sufficient to prevent capsules from separating. We now systematically decrease $A^{\text{cap-att}}$ and analyze the outcomes of simulations as before. In Figure 6, we present a phase map showing the behavior of the capsules at different

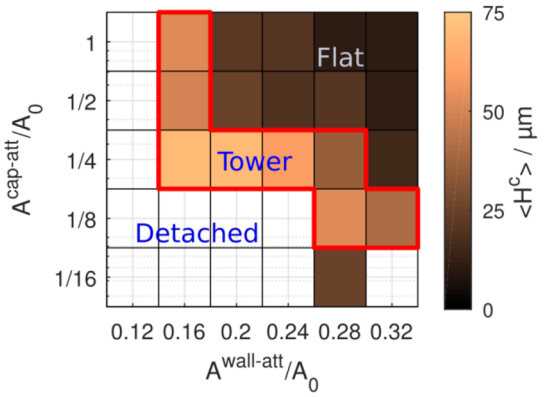

Figure 6. Phase map of assembly outcomes as capsule–wall and capsule–capsule attractions are varied. Stable towers formed in at least two out of three simulation runs for the parameter combinations enclosed by the thick, red line. Below this region, the capsules detached from the wall (and $\langle H^C \rangle$ generally could not be defined), whereas above this region, the capsules were firmly attached to the wall and the resulting structure was flat rather than tower-like.

combinations of $A^{\text{wall-att}}$ and $A^{\text{cap-att}}$. As $A^{\text{cap-att}}$ decreases from the baseline value $A^{\text{cap-att}} = A_0$, the capsules become less rigidly attached to the cluster. It is observed that the capsules rearrange more readily within the cluster without detaching. The diffusioosmotic flow above the catalytic patch tends to lift the capsules up, stretching the cluster into a taller structure (see Video SV5). This effect results in towers forming at much higher values of $A^{\text{wall-att}}$ that previously gave only flat structures. When $A^{\text{cap-att}}$ is decreased further, the attraction between the capsules becomes too weak and the capsules are pulled apart by the diffusioosmotic flow. Hence, the capsules detach from the cluster once they are pushed onto the nonattractive central patch on the wall (see Video SV6).

Towers formed robustly in 8 of 30 tested parameter combinations, indicating that there is some flexibility in the choice of parameters that will achieve this outcome. We note, however, that the region of phase space in which towers formed is relatively thin. Small deviations in $A^{\text{wall-att}}$ and $A^{\text{cap-att}}$ in particular phase space directions could result in the detachment of the capsules or formation of flat clusters.

3.5. Surface Attraction Patterning to Control Morphology. As discussed in section 3.2, the motion of the capsules along the surface can be altered by patterning the surface with attractive and nonattractive regions. It is energetically more favorable for the capsules to remain over attractive regions. We exploited this behavior to organize the aggregating capsules into spiral queues. As shown in Figure 7A, we used a nonattractive pattern consisting of four spirals in a slightly larger domain, $L = 200$ μm, $H = 100$ μm. The capsules moved toward the center of the pattern, under the action of the diffusioosmotic flow, until one of the nonattractive spiral arms was encountered. The capsules then moved along the edge of the spiral arm to the cusp at the intersection with the neighboring nonattractive spiral arm. The purpose of these spiral arms is to funnel the capsules into discrete, well-defined streams. With this pattern, the capsules tended to arrive at the cusps in a single file. The energy barrier associated with leaving the attractive region of the surface held the capsules at the cusps until they were pushed off by the incoming capsules (Video SV7).

DOI: 10.1021/acs.langmuir.7b04051
Langmuir 2018, 34, 2890–2899

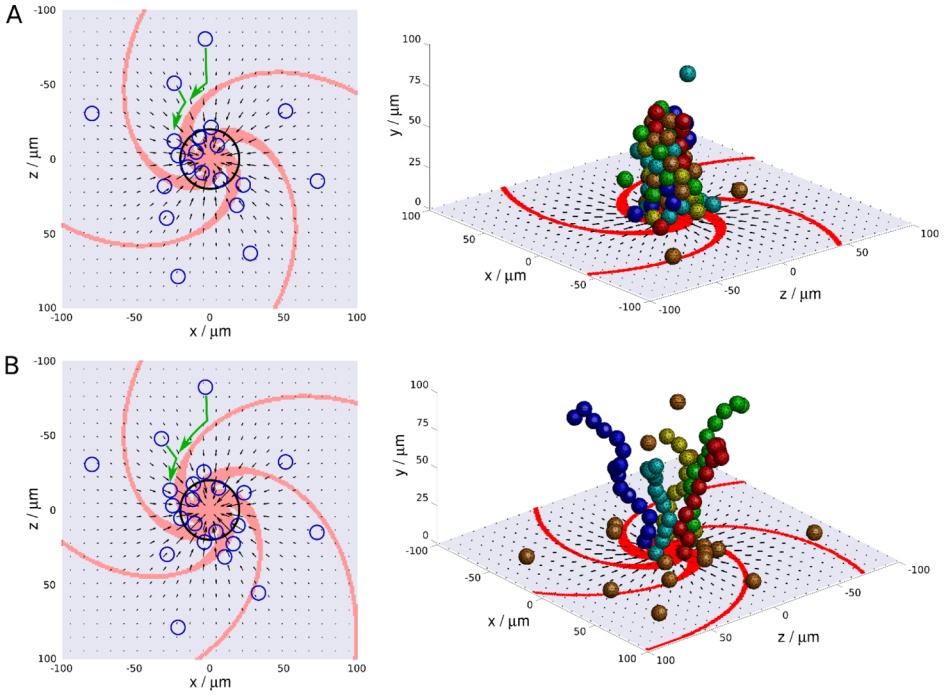

Figure 7. Assembly on spiraling nonattractive wall patterns. Light gray portions of the wall are attractive to capsules, whereas red portions are nonattractive. The black arrows indicate the direction and relative speed of the fluid flow close to the wall. Top-down views of the pattern are shown on the left-hand side. The formation of queues of capsules (small rings) along the spiral arms is illustrated schematically. The large, circular ring marks the perimeter of the catalytic patch. (A,B) correspond to simulations with different nonattractive patterns. Apart from the number of spiral arms, the two patterns differ in the distance between the capsules in adjacent queues. In (A), this distance is smaller and allows capsules in all queues to join together. In (B), the capsules are kept further away from adjacent queues. The right-hand side shows the final configuration of clusters assembled on these patterns. A single tower forms in (A), whereas the capsules are arranged into five separate strands in (B). The evolution of these structures is presented in Video SV6 and SV7.

In Figure 7A, the pattern was designed so that neighboring cusps were approximately one capsule diameter apart. This proximity allowed capsules from the adjacent streams to come into contact and stick together as they detached from the wall, resulting in towers. The cusps in the surface pattern serve as anchor points for the tower; the cluster remains attached to the surface through the capsules that occupy the cusps.

A modified pattern was used for the simulation shown in Figure 7B, leading to a very different assembled structure. The distinguishing feature of the pattern in this scenario is that the cusps of the attractive regions were further apart than in the pattern from Figure 7A. The capsules traveled along the spiral arms and detached from the wall at the cusps as before. With a greater spacing between the cusps, however, the capsules remained separated from the capsules in adjacent streams. Instead of merging together to form a tower, the capsules assembled into independent filaments. These filaments spread apart from each other because the fluid flow diverges from the vertical axis (see Figure 2, Video SV8).

4. CONCLUSIONS

We described a novel method for directing the assembly of spherical microcapsules into 3D, tower-like structures and filaments. The aggregation of the microcapsules, which are initially dispersed over a surface, is driven by a diffusioosmotic flow along the surface toward a catalytic patch. Patterned functionalization of the surface is used to control where the capsules are arrested and to anchor the 3D structure to the surface. We demonstrated that the strength of capsule−wall attractions can be tuned so that the capsules remain attached to these designated sites until other capsules arrived to take their place. Thus, the structures grow upward as new capsules are inserted between the surface and the existing structure.

Unexpectedly, we observed that the strength of capsule−capsule attractions also influenced the detachment of capsules from the wall; for higher values of $A^{\text{cap-att}}$, clusters remained attached to the wall at lower values of $A^{\text{wall-att}}$. Hence, $A^{\text{wall-att}}$ and $A^{\text{cap-att}}$ must be tuned simultaneously to ensure that the capsules remain cohesive and connected to the wall while allowing the fluid flow to pull the cluster into a tall, out-of-plane structure.

In our simulations, we adopted periodic boundary conditions for the chemical concentrations and fluid flow on the lateral domain boundaries. This setup approximates a physical system with a large, square lattice of catalytic patches on the bottom surface. Diffusioosmosis drives the fluid flow, and the capsules, toward the nearest patch. A tower, or a set of filaments, would form at each patch. Thus, many clusters can be assembled simultaneously in one chamber.

Notably, we utilized spherical particles with no intrinsic anisotropy; this contrasts with previously reported systems that used asymmetry in shape and surface functionalization to assemble anisotropic structures.[46−48] Apart from being simpler to manufacture, one advantage of using isotropic particles is that the structures they form are not dictated by the fixed design of the particle. The same particles could be assembled into different morphologies, potentially concurrently at different locations on the surface.

Finally, we remark that the stability of the assembled structures depends on the interactions between the capsules. If

DOI: 10.1021/acs.langmuir.7b04051
Langmuir 2018, 34, 2890−2899

the fluid flow were to change or cease after the assembly of a tower, the capsules could detach or rearrange to form a new shape. A sequence of flow fields, driven by different catalytic patches, could be used to manipulate the structures and form more complex morphologies. Capsules could be dispersed by weakening the interparticle attraction through changes in temperature, for instance.[49] Conversely, strengthening the attraction between the capsules would stabilize the structures. Capsules can be locked in place once the final configuration is achieved, as in the fabrication of colloidosomes.[50] Our method of flow-directed assembly, combined with dynamically tunable interparticle interactions, could form the basis for constructing a variety of reconfigurable structures from simple subunits.

■ ASSOCIATED CONTENT

Supporting Information

The Supporting Information is available free of charge on the ACS Publications website at DOI: 10.1021/acs.langmuir.7b04051.

The following files are available free of charge. In all videos, fluid flows are visualized in the $z = 0$ plane on the left (side view) and in the $y = 0.5$ μm plane on the right (top-down view). Blue color indicates the regions of high flow speed. The red background pattern in the top-down view is the nonattractive portion of the surface. Formation of a tower using attractive and repulsive interactions based on positions of capsule centers instead of surface nodes; aggregation and detachment of capsules; formation of the tower; formation of the "flat" structure; formation of a tower with a lower capsule attraction; aggregation and detachment of capsules with a lower capsule attraction; formation of a tower on a spiral nonattractive pattern; and formation of a multiple filaments on a spiral nonattractive pattern (ZIP)

■ AUTHOR INFORMATION

Corresponding Authors

*E-mail: henry.shum@uwaterloo.ca (H.S.).
*E-mail: balazs@pitt.edu (A.C.B.).

ORCID

Anna C. Balazs: 0000-0002-5555-2692

Notes

The authors declare no competing financial interest.

■ ACKNOWLEDGMENTS

A.C.B. gratefully acknowledges funding from the NSF CCI Phase I: Center for Chemo-mechanical Assembly.

■ REFERENCES

(1) Kolmakov, G. V.; Yashin, V. V.; Levitan, S. P.; Balazs, A. C. Designing Communicating Colonies of Biomimetic Microcapsules. *Proc. Natl. Acad. Sci. U.S.A.* **2010**, *107*, 12417−12422.

(2) Yashin, V. V.; Kolmakov, G. V.; Shum, H.; Balazs, A. C. Designing Synthetic Microcapsules That Undergo Biomimetic Communication and Autonomous Motion. *Langmuir* **2015**, *31*, 11951−11963.

(3) Shum, H.; Yashin, V. V.; Balazs, A. C. Self-Assembly of Microcapsules Regulated via the Repressilator Signaling Network. *Soft Matter* **2015**, *11*, 3542−3549.

(4) Shklyaev, O. E.; Shum, H.; Sen, A.; Balazs, A. C. Harnessing Surface-Bound Enzymatic Reactions to Organize Microcapsules in Solution. *Sci. Adv.* **2016**, *2*, No. e1501835.

(5) Shklyaev, O. E.; Shum, H.; Yashin, V. V.; Balazs, A. C. Convective Self-Sustained Motion in Mixtures of Chemically Active and Passive Particles. *Langmuir* **2017**, *33*, 7873−7880.

(6) Reuss, F. F. Charge-Induced Flow. *Proceedings of the Imperial Society of Naturalists of Moscow*, 1809; Vol. 3, pp 327−344.

(7) Gu, Y.; Li, D. The ζ-Potential of Glass Surface in Contact with Aqueous Solutions. *J. Colloid Interface Sci.* **2000**, *226*, 328−339.

(8) Sze, A.; Erickson, D.; Ren, L.; Li, D. Zeta-Potential Measurement Using the Smoluchowski Equation and the Slope of the Current−time Relationship in Electroosmotic Flow. *J. Colloid Interface Sci.* **2003**, *261*, 402−410.

(9) Rice, C. L.; Whitehead, R. Electrokinetic Flow in a Narrow Cylindrical Capillary. *J. Phys. Chem.* **1965**, *69*, 4017−4024.

(10) Anderson, J. L. Colloid Transport by Interfacial Forces. *Annu. Rev. Fluid Mech.* **1989**, *21*, 61−99.

(11) Manz, A.; Effenhauser, C. S.; Burggraf, N.; Harrison, D. J.; Seiler, K.; Fluri, K. Electroosmotic Pumping and Electrophoretic Separations for Miniaturized Chemical Analysis Systems. *J. Micromech. Microeng.* **1994**, *4*, 257.

(12) Takamura, Y.; Onoda, H.; Inokuchi, H.; Adachi, S.; Oki, A.; Horiike, Y. Low-Voltage Electroosmosis Pump for Stand-Alone Microfluidics Devices. *Electrophoresis* **2003**, *24*, 185−192.

(13) Keh, H. J.; Wu, J. H. Electrokinetic Flow in Fine Capillaries Caused by Gradients of Electrolyte Concentration. *Langmuir* **2001**, *17*, 4216−4222.

(14) Keh, H. J.; Ma, H. C. Diffusioosmosis of Electrolyte Solutions along a Charged Plane Wall. *Langmuir* **2005**, *21*, 5461−5467.

(15) Hoshyargar, V.; Ashrafizadeh, S. N.; Sadeghi, A. Diffusioosmotic Flow in Rectangular Microchannels. *Electrophoresis* **2016**, *37*, 809−817.

(16) McDermott, J. J.; Kar, A.; Daher, M.; Klara, S.; Wang, G.; Sen, A.; Velegol, D. Self-Generated Diffusioosmotic Flows from Calcium Carbonate Micropumps. *Langmuir* **2012**, *28*, 15491−15497.

(17) Yadav, V.; Zhang, H.; Pavlick, R.; Sen, A. Triggered "On/Off" Micropumps and Colloidal Photodiode. *J. Am. Chem. Soc.* **2012**, *134*, 15688−15691.

(18) Ibele, M. E.; Wang, Y.; Kline, T. R.; Mallouk, T. E.; Sen, A. Hydrazine Fuels for Bimetallic Catalytic Microfluidic Pumping. *J. Am. Chem. Soc.* **2007**, *129*, 7762−7763.

(19) Esplandiu, M. J.; Afshar Farniya, A.; Bachtold, A. Silicon-Based Chemical Motors: An Efficient Pump for Triggering and Guiding Fluid Motion Using Visible Light. *ACS Nano* **2015**, *9*, 11234−11240.

(20) Michler, D.; Shahidzadeh, N.; Sprik, R.; Bonn, D. Directed Vesicle Transport by Diffusio-Osmosis. *Europhys. Lett.* **2015**, *110*, 28001.

(21) Niu, R.; Oğuz, E. C.; Müller, H.; Reinmüller, A.; Botin, D.; Löwen, H.; Palberg, T. Controlled Assembly of Single Colloidal Crystals Using Electro-Osmotic Micro-Pumps. *Phys. Chem. Chem. Phys.* **2017**, *19*, 3104−3114.

(22) Hammer, D. A.; Robbins, G. P.; Haun, J. B.; Lin, J. J.; Qi, W.; Smith, L. A.; Ghoroghchian, P. P.; Therien, M. J.; Bates, F. S. Leuko-Polymersomes. *Faraday Discuss.* **2008**, *139*, 129−141.

(23) Santore, M. M.; Kozlova, N. Micrometer Scale Adhesion on Nanometer-Scale Patchy Surfaces: Adhesion Rates, Adhesion Thresholds, and Curvature-Based Selectivity. *Langmuir* **2007**, *23*, 4782−4791.

(24) Letteri, R. A.; Santa Chalarca, C. F.; Bai, Y.; Hayward, R. C.; Emrick, T. Forming Sticky Droplets from Slippery Polymer Zwitterions. *Adv. Mater.* **2017**, *29*, 1702921.

(25) Milam, V. T.; Hiddessen, A. L.; Crocker, J. C.; Graves, D. J.; Hammer, D. A. DNA-Driven Assembly of Bidisperse, Micron-Sized Colloids. *Langmuir* **2003**, *19*, 10317−10323.

(26) Chen, S.; Doolen, G. D. Lattice Boltzmann Method for Fluid Flows. *Annu. Rev. Fluid Mech.* **1998**, *30*, 329−364.

(27) Ladd, A. J. C.; Verberg, R. Lattice-Boltzmann Simulations of Particle-Fluid Suspensions. *J. Stat. Phys.* **2001**, *104*, 1191−1251.

(28) Guo, Z.; Zheng, C.; Shi, B. Discrete Lattice Effects on the Forcing Term in the Lattice Boltzmann Method. *Phys. Rev. E: Stat., Nonlinear, Soft Matter Phys.* **2002**, *65*, 046308.

DOI: 10.1021/acs.langmuir.7b04051
Langmuir 2018, 34, 2890−2899

(29) Aidun, C. K.; Clausen, J. R. Lattice-Boltzmann Method for Complex Flows. *Annu. Rev. Fluid Mech.* **2010**, *42*, 439−472.
(30) Peskin, C. S. Numerical Analysis of Blood Flow in the Heart. *J. Comput. Phys.* **1977**, *25*, 220−252.
(31) Peskin, C. S. The Immersed Boundary Method. *Acta Numer.* **2002**, *11*, 479−517.
(32) Feng, Z.-G.; Michaelides, E. E. The Immersed Boundary-Lattice Boltzmann Method for Solving Fluid−particles Interaction Problems. *J. Comput. Phys.* **2004**, *195*, 602−628.
(33) Bringley, T. T.; Peskin, C. S. Validation of a Simple Method for Representing Spheres and Slender Bodies in an Immersed Boundary Method for Stokes Flow on an Unbounded Domain. *J. Comput. Phys.* **2008**, *227*, 5397−5425.
(34) Liu, Y.; Zhang, L.; Wang, X.; Liu, W. K. Coupling of Navier−Stokes Equations with Protein Molecular Dynamics and Its Application to Hemodynamics. *Int. J. Numer. Methods Fluids* **2004**, *46*, 1237−1252.
(35) Alexeev, A.; Verberg, R.; Balazs, A. C. Modeling the Motion of Microcapsules on Compliant Polymeric Surfaces. *Macromolecules* **2005**, *38*, 10244−10260.
(36) Zhang, J.; Johnson, P. C.; Popel, A. S. An Immersed Boundary Lattice Boltzmann Approach to Simulate Deformable Liquid Capsules and Its Application to Microscopic Blood Flows. *Phys. Biol.* **2007**, *4*, 285−295.
(37) Hamaker, H. C. The London−van Der Waals Attraction between Spherical Particles. *Physica* **1937**, *4*, 1058−1072.
(38) Pantina, J. P.; Furst, E. M. Elasticity and Critical Bending Moment of Model Colloidal Aggregates. *Phys. Rev. Lett.* **2005**, *94*, 138301.
(39) Özişik, M. N. *Finite Difference Methods in Heat Transfer*; CRC Press: Boca Raton, 1994.
(40) Thomas, J. W. *Numerical Partial Differential Equations: Finite Difference Methods*; Springer Verlag: New York, 1995.
(41) Sengupta, S.; Patra, D.; Ortiz-Rivera, I.; Agrawal, A.; Shklyaev, S.; Dey, K. K.; Córdova-Figueroa, U.; Mallouk, T. E.; Sen, A. Self-Powered Enzyme Micropumps. *Nat. Chem.* **2014**, *6*, 415−422.
(42) Das, S.; Shklyaev, O. E.; Altemose, A.; Shum, H.; Ortiz-Rivera, I.; Valdez, L.; Mallouk, T. E.; Balazs, A. C.; Sen, A. Harnessing Catalytic Pumps for Directional Delivery of Microparticles in Microchambers. *Nat. Commun.* **2017**, *8*, 14384.
(43) Niu, R.; Kreissl, P.; Brown, A. T.; Rempfer, G.; Botin, D.; Holm, C.; Palberg, T.; de Graaf, J. Microfluidic Pumping by Micromolar Salt Concentrations. *Soft Matter* **2017**, *13*, 1505−1518.
(44) Hong, Y.; Diaz, M.; Córdova-Figueroa, U. M.; Sen, A. Light-Driven Titanium-Dioxide-Based Reversible Microfireworks and Micromotor/Micropump Systems. *Adv. Funct. Mater.* **2010**, *20*, 1568−1576.
(45) Godin, M.; Bryan, A. K.; Burg, T. P.; Babcock, K.; Manalis, S. R. Measuring the Mass, Density, and Size of Particles and Cells Using a Suspended Microchannel Resonator. *Appl. Phys. Lett.* **2007**, *91*, 123121.
(46) Furst, E. M. Colloidal Self-Assembly: Reversible Actuation. *Nat. Mater.* **2015**, *14*, 19−20.
(47) Wolters, J. R.; Avvisati, G.; Hagemans, F.; Vissers, T.; Kraft, D. J.; Dijkstra, M.; Kegel, W. K. Self-Assembly of "Mickey Mouse" Shaped Colloids into Tube-like Structures: Experiments and Simulations. *Soft Matter* **2015**, *11*, 1067−1077.
(48) Shah, A. A.; Schultz, B.; Zhang, W.; Glotzer, S. C.; Solomon, M. J. Actuation of Shape-Memory Colloidal Fibres of Janus Ellipsoids. *Nat. Mater.* **2015**, *14*, 117−124.
(49) Leunissen, M. E.; Dreyfus, R.; Cheong, F. C.; Grier, D. G.; Sha, R.; Seeman, N. C.; Chaikin, P. M. Switchable Self-Protected Attractions in DNA-Functionalized Colloids. *Nat. Mater.* **2009**, *8*, 590−595.
(50) Dinsmore, A. D.; Hsu, M. F.; Nikolaides, M. G.; Marquez, M.; Bausch, A. R.; Weitz, D. A. Colloidosomes: Selectively Permeable Capsules Composed of Colloidal Particles. *Science* **2002**, *298*, 1006−1009.

DOI: 10.1021/acs.langmuir.7b04051
Langmuir 2018, 34, 2890−2899